Nonmonotonic $d_{x^2-y^2}$ Superconducting Order Parameter in $Nd_{2-x}Ce_xCuO_4$

G. Blumberg,[1,*] A. Koitzsch,[1] A. Gozar,[1] B. S. Dennis,[1] C. A. Kendziora,[2] P. Fournier,[3,†] and R. L. Greene[3]

[1]Bell Laboratories, Lucent Technologies, Murray Hill, New Jersey 07974
[2]United States Naval Research Laboratory, Code 6333, Washington, D.C. 20375
[3]Center for Superconductivity Research and Department of Physics, University of Maryland, College Park, Maryland 20742
(Received 15 June 2001; published 26 February 2002)

Low energy polarized electronic Raman scattering of the electron-doped superconductor $Nd_{2-x}Ce_xCuO_4$ ($x = 0.15$, $T_c = 22$ K) has revealed a *nonmonotonic* $d_{x^2-y^2}$ superconducting order parameter. It has a maximum gap of $4.4k_BT_c$ at Fermi surface intersections with an antiferromagnetic Brillouin zone (the "hot spots") and a smaller gap of $3.3k_BT_c$ at fermionic Brillouin zone boundaries. The gap enhancement in the vicinity of the hot spots emphasizes the role of antiferromagnetic fluctuations and the similarity in the origin of superconductivity for electron- and hole-doped cuprates.

Introduction.—$Nd_{2-x}Ce_xCuO_4$ (NCCO) is one of a few electron-doped cuprate superconductors [1]. The physical properties of the electron-doped cuprates are different from the hole doped. Structurally, NCCO does not have apical oxygen atoms. It is commonly believed that the charge carriers in NCCO are electrons rather than holes as in other cuprate families [1,2]. In optimally hole-doped cuprates the normal state resistivity increases linearly over a wide range of temperatures, while for NCCO the in-plane resistivity is quadratic in temperature with a large residual value [3]. For the electron-doped cuprates the superconducting (SC) transition temperature is relatively low and the superconductivity occurs in a narrow doping range [1]. From the early tunneling [4] and microwave measurements an *s*-wave SC order parameter (OP) was suggested [5] that is in contrast with the *d*-wave symmetry established for hole-doped compounds. The early Raman measurements were interpreted as evidence for a nearly uniformly gapped Fermi surface (FS) [6] consistent with the *s*-wave OP. However, the interpretation of more recent microwave measurements [7,8] along with angle-resolved photoemission spectroscopy (ARPES) [9,10] and phase sensitive scanning SQUID microscope experiments [11] is consistent with *d*-wave OP.

We report polarized low energy electronic Raman scattering studies on NCCO single crystals and show that the data are consistent with a SC OP of the $d_{x^2-y^2}$ symmetry. However, as distinguished from the simplest commonly assumed SC gap function, $\Delta(\mathbf{k}) \propto \cos(k_x a) - \cos(k_y a)$, where $\mathbf{k}$ is a wave vector on the FS and a is the ab-plane lattice constant, the present results require a *nonmonotonic* form of the OP. We find that in contrast with hole-doped cuprates for NCCO the positions of the SC gap maxima are located closer to the nodes than to the Brillouin zone (BZ) boundaries. The gap opens up rapidly with departure from the diagonal nodal directions and quickly reaches its maximum value of $4.4k_BT_c$ at the intersections of the FS and the antiferromagnetic (AF) BZ. However, the gap value drops to $3.3k_BT_c$ at the BZ boundaries. The implications

of such *nonmonotonic* OP to the doping dependence of T_c are discussed.

Experimental.—The Raman experiments were performed from a natural ab surface of a platelike single crystal grown as described in Ref. [12]. After growth, the crystal was annealed in an oxygen-reduced atmosphere to induce the doping level for optimal T_c. SC transition measured by SQUID was about 22 K with a width of about 2 K. The sample was mounted in an optical continuous helium flow cryostat. Spectra were taken in a backscattering geometry using linearly polarized excitations of a Kr^+ laser from near infrared to violet. An incident laser power less than 2 mW was focused to a 50 μm spot onto the sample surface. The referred temperatures were corrected for laser heating. The spectra were measured at temperatures between 5 and 35 K and were analyzed by a custom triple grating spectrometer. The data were corrected for the spectral response of the spectrometer and for the optical properties of the material at different wavelengths as described in Ref. [13].

The polarization directions of the incident ($\mathbf{e}_i$) and scattered ($\mathbf{e}_s$) photons are indicated by ($\mathbf{e}_i, \mathbf{e}_s$) with $x = [100]$, $y = [010]$, $x' = [110]$, and $y' = [\bar{1}10]$. The presented data were taken in (xy), $(x'y')$, and (xx) scattering geometries. For tetragonal D_{4h} symmetry these geometries correspond to spectra of $B_{2g} + A_{2g}$, $B_{1g} + A_{2g}$, and $A_{1g} + B_{1g}$ representations. In addition, by using geometries with circularly polarized light we checked the intensity of the A_{2g} component and found it to be negligibly weak.

Raman scattering symmetries.—The electronic Raman response function for a given geometry ($\mathbf{e}_i, \mathbf{e}_s$) is proportional to the sum over the density of states at the FS weighted by the momentum $\mathbf{k}$ dependent form factor [14–16]. By choosing the scattering geometries one can selectively probe different regions of the FS and obtain information about the $\mathbf{k}$ dependence of the SC OP. For the B_{1g} channel the Raman spectrum has a form factor of $d_{x^2-y^2}$ symmetry that vanishes at the $(0,0) \rightarrow (\pi, \pi)$ and

the equivalent diagonal lines of the BZ (see Fig. 1). The spectrum intensity in the B_{1g} channel integrates mainly from the regions of the FS distant from these diagonals, near intersections of the FS and the BZ boundary (ZB). In contrast, the form factor for the B_{2g} spectrum has d_{xy} symmetry and therefore vanishes along $(0,0) \rightarrow (0,\pi)$ and the equivalent lines. The intensity in the B_{2g} channel is mainly determined by excitations near $(\pi/2, \pi/2)$ and the equivalent points. All regions of momentum space may contribute to the fully symmetric A_{1g} channel [21].

The pair breaking excitations.— In Fig. 2 we compare the low energy Raman spectra above and below the SC transition taken with the excitation energy $\omega_L = 1.9$ eV for three symmetry representations: B_{1g}, B_{2g}, and A_{1g}. Above T_c spectra exhibit a flat electronic Raman continuum. In the SC state the low-frequency tail of the Raman continuum changes to reflect the opening of the SC gap: the strength of the low-frequency continuum is reduced and the spectrum acquires the so-called 2Δ peak as a result of excitations across the anisotropic gap, $2\Delta(\mathbf{k})$. These peaks correspond to the excitations out of the SC condensate. For different scattering geometries spectra differ in their intensity as well as in the position of the 2Δ peaks. The peaks in the A_{1g} and B_{2g} channels are an order of magnitude stronger than in the B_{1g} channel. For B_{2g} symmetry the

peak is at the highest energy, at about 67 cm^{-1}, followed by the peaks in B_{1g} and A_{1g} channels at 50 and 40 cm^{-1} correspondingly.

These results are in sharp contrast to the hole-doped cuprates where the most prominent scattering is observed in the B_{1g} channel for which the 2Δ peak is at the highest frequency [22–28]. For the hole-doped cuprates the interpretation of Raman data is consistent with $d_{x^2-y^2}$ SC OP of the simplest *monotonic* $\propto \sin(2\phi)$ form shown in Fig. 1B. The role of orthorhombic distortions and impurities has been discussed in Refs. [16,29–31].

The earlier low-temperature Raman data from NCCO were measured down to about 25 cm^{-1} with $\omega_L = 2.6$ eV [6]. The data exhibited a strong residual scattering intensity. The observed 2Δ peak in the B_{1g} channel started at a threshold from the low energy side. The authors discuss possible experimental artifacts for the residual intensity and suggest that the observed threshold supports an anisotropic s-wave gap interpretation (see Fig. 1B). Our data extend to much lower frequencies (Figs. 2 and 3). The spectra for all scattering channels show a smoothly dropping intensity below the 2Δ peak down to the lowest energies measured. Based on our data we exclude the anisotropic s-wave interpretation since any fully gapped FS would lead to a Raman intensity threshold as it has been observed for classical superconductors [14]. The smooth decrease of the scattering intensity is a signature of the nodes in the OP [25].
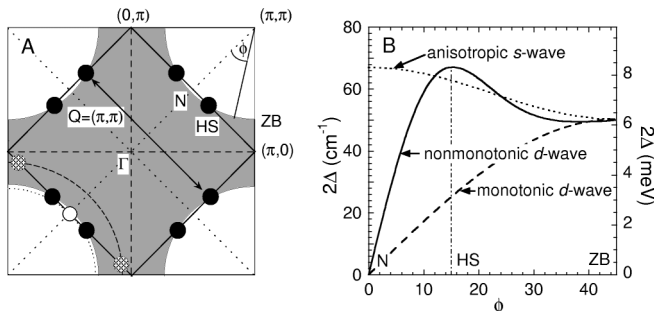

FIG. 1. (A) A schematic representation of the electron-doped FS of NCCO [17]. The occupied electron states are shaded. The AF BZ at half filling is shown as the square rotated by 45°. AF fluctuations enhance interactions between fermions around the "hot spots" (filled circles), the regions of the FS connected by the $\mathbf{Q} = (\pi, \pi)$ vector [18]. The location of the hot spots sensitively depend on the doping level. The FS shrinks with further electron doping until the intersection with the AF BZ vanishes (dotted lines and empty circle in the lower left quadrant). The hole-doped cuprates exhibit a large FS with the hot spots shifted to the vicinity of $(\pi, 0)$ and the equivalent points (dashed lines and hatched circles in the lower left quadrant) [19,20]. The dotted diagonal (dashed horizontal and vertical) lines denote the nodes of the B_{1g} (B_{2g}) Raman form factor. (B) The magnitude of the $d_{x^2-y^2}$ OP as a function of the angle ϕ along the FS. Solid line: *nonmonotonic* OP for NCCO. The gap value rises rapidly from the nodal diagonal direction (N) to its maximum value $2\Delta = 67$ cm^{-1} at the hot spot (HS) observed in the B_{2g} channel. The 2Δ peak at 50 cm^{-1} in the B_{1g} channel corresponds to the value at the BZ boundary (ZB). Dashed line: *monotonic* $\sin(2\phi)$ form. Dotted line: anisotropic s-wave OP proposed in Ref. [6].
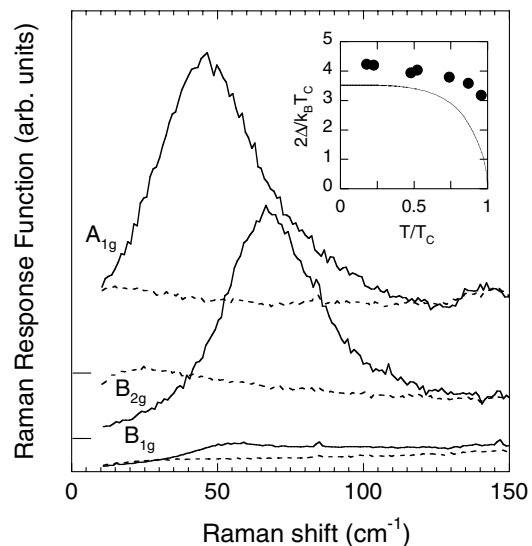

FIG. 2. Low-frequency Raman scattering spectra with 1.9 eV excitation for different symmetry channels. The solid lines denote spectra at 11 K in the SC state and the dashed lines denote spectra taken above T_c at 35 K. The baselines are shifted as indicated by the ticks. The B_{1g} spectra correspond to $x'y'$, the B_{2g} to xy, and the A_{1g} to $xx - x'y'$ scattering geometries. The inset shows the temperature evolution of the 2Δ-peak energy in the B_{2g} channel. The line indicates the mean field BCS temperature dependence.
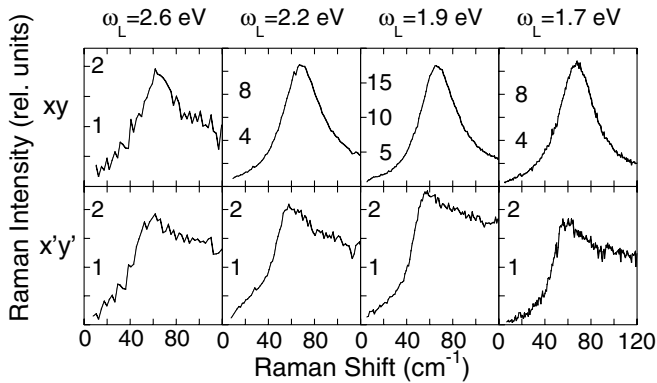
FIG. 3. Low energy Raman spectra at 8 K in the B_{2g} (xy) and B_{1g} ($x'y'$) channels for excitations from blue to near IR. Note that for shorter wavelength excitations the intensities of the 2Δ peaks in two channels are comparable, while for the red excitations the intensities in the B_{2g} channel are an order of magnitude stronger than in the B_{1g} channel.

The gap anisotropy.—The observation of the 2Δ peak in the B_{2g} channel at energies higher than in the B_{1g} channel suggests a *nonmonotonic* OP with maxima in $\Delta(\mathbf{k})$ closer to the $(0,0) \rightarrow (\pi,\pi)$ diagonal than to the BZ boundary. The recent ARPES studies of NCCO exhibit a node in $\Delta(\mathbf{k})$ along this diagonal direction [9,10]. Our Raman data can be reconciled with the ARPES results by including higher harmonics, like $\sin(6\phi)$, to the *monotonic* $\sin(2\phi)$ form of the $d_{x^2-y^2}$ OP. The resulting *nonmonotonic* form is shown in Fig. 1B. In Fig. 1A we sketch the FS as seen by ARPES [17]. The latter data exhibit regions of suppressed spectral weight at the intersections with the AF BZ boundary, a behavior similar to the destruction of the FS at the hot spots in the pseudogap phase seen in hole-doped cuprates [19,20]. Strong AF fluctuations are believed to be responsible for such hot spot behavior [18,32–35].

We assume that the AF interactions are responsible for the SC coupling mechanism and that as in the hole-doped cuprates the SC gap reaches its maximum value in the vicinity of the hot spots. For the hole-doped cuprates with a large FS the hot spots are close to the BZ boundary. For electron-doped cuprates the position of the hot spots sensitively depends on the size of the FS and, hence, on the amount of doping. As is seen in the ARPES data [17] for the optimally doped NCCO, the hot spots are close to the BZ diagonals and therefore in Raman the maximum gap value appears in the B_{2g} channel. The peak position at about 67 cm^{-1} is consistent with the maximum gap value of 3.7 meV observed in tunneling spectroscopy [4]. The 2Δ peak in the B_{1g} channel reflects the gap magnitude at the BZ boundary (see Fig. 1B). Indeed, the peak position at about $2\Delta_{B_{1g}} = 50$ cm^{-1} corresponds to 3 meV for a single $\Delta(\mathbf{k}_{ZB})$ that is consistent with the leading edge gap estimates between 1.5 and 3 meV at the BZ boundary by ARPES [9,10]. For slightly stronger electron doping

the intersection of the AF BZ and the FS disappears. This naturally explains the narrow doping range for superconductivity in the electron-doped cuprates.

The superconducting gap temperature dependence.—In the inset in Fig. 2 we show the temperature development of the 2Δ-peak position in the B_{2g} channel. The SC gap opens up very rapidly with cooling below T_c and soon approaches its maximum value $4.4k_BT_c$ which is within the margin of the strong coupling limit and is close to the gap value observed for heavily hole overdoped cuprates. Optimally and especially hole-underdoped cuprates exhibit much larger gap values [27,28].

The resonant Raman excitation profile.—We performed a systematic study of the Raman scattering efficiency as a function of the excitation photon energy. The low frequency response at 8 K in the B_{1g} and B_{2g} channels for excitations from blue to near IR are shown in Fig. 3. For the blue excitation ($\omega_L = 2.6$ eV) our data are consistent with the earlier results of Ref. [6] showing comparable intensities in both B_{1g} and B_{2g} channels. The relative intensities change drastically when the excitation energy is decreased below 2.5 eV. While the peak in the B_{1g} channel only slightly increases in intensity, the peak in the B_{2g} channel rapidly increases by an order of magnitude and exhibits a maximum around excitation $\omega_L = 1.9$ eV. The resonance profiles of the 2Δ peak for both B_{1g} and B_{2g} channels are presented in Fig. 4A and are compared with optical conductivity data [36] that exhibit a band between 1.7 and 2.5 eV. This band has been ascribed to the charge-transfer process between the fully occupied oxygen $2p$ band and the upper Hubbard band (UHB) [37] that has been suggested to be a doubly occupied hybridized oxygen $2p$ and a copper $3d$ state.

In Fig. 4B we show a schematic diagram for the resonant Raman scattering process in strongly correlated electron-doped cuprates. The lower Hubbard band (LHB) and the
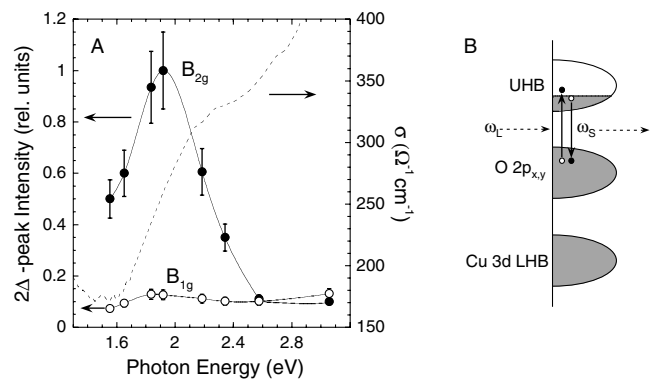

FIG. 4. (A) Intensity of the 2Δ peaks at 8 K in the B_{1g} (○) and B_{2g} (●) channels as a function of the excitation photon energy ω_L compared to the optical conductivity data (dashed line) at 300 K [36]. The solid lines are guides to the eye. (B) A schematic diagram for the resonant electronic Raman scattering process in electron-doped cuprates.

oxygen band above are fully occupied. Doped electrons shift the Fermi energy to the UHB. Resonant enhancement of the Raman scattering process occurs when the energy of the incoming or scattered photons, or both, are in resonance with the interband transitions. Our results imply that the intermediate state for the Raman process is the same state which is seen near 2.1 eV in the optical conductivity. Moreover, because the observed resonance enhancement for the B_{2g} channel is much stronger than for the B_{1g} channel we anticipate that the interband transition occurs near the $(\pi/2, \pi/2)$ point. Angle-resolved valence-band photoemission spectra indeed exhibit a band that is peaked at this point at about 2.6 eV below the Fermi energy [10]. The excitation out of this band to the UHB may originate the 2.1 eV transition in the optical conductivity. A slight downscale in energy reflects the final state interactions.

Summary.—Low energy electronic Raman scattering has been investigated for NCCO single crystals and the role of interband transitions for the resonant Raman coupling has been discussed. The low temperature data for different scattering channels have been found to be consistent with a *nonmonotonic* functional form of the $d_{x^2-y^2}$ OP. The SC gap opens up rapidly with departure from the nodal directions and reaches its maximum value of $4.4k_BT_c$ at the hot spots that are located closer to the nodes than to the BZ boundaries where the gap value drops to $3.3k_BT_c$. The enhancement of the gap value in the proximity of the hot spots emphasizes the role of AF fluctuations for the superconductivity in the electron-doped cuprates. Despite the strong differences between the electron- and hole-doped cuprates, their superconductivity appears to share the same symmetry and a similar origin.

---

*To whom correspondence should be addressed.
　Email address: girsh@bell-labs.com
†Permanent address: Centre de Recherche sur Les Propriétés Électroniques de Matériaux Avancés et Département de Physique, Université de Sherbrooke, Sherbrooke, Québec, Canada, J1K 2R1.

[1] Y. Tokura, H. Takagi, and S. Uchida, Nature (London) **377**, 345 (1989); H. Takagi, S. Uchida, and Y. Tokura, Phys. Rev. Lett. **62**, 1197 (1989).

[2] The assignment of electrons as the charge carriers is based on the negative value of the Hall coefficient. However, there is evidence for both electron and hole carriers in the temperature dependence of the Hall coefficient and a two band model with electrons and holes acting as charge carriers has been proposed to account for this less than trivial behavior. Wu Jiang *et al.,* Phys. Rev. Lett. **73**, 1291 (1994); S. I. Woods *et al.,* Phys. Rev. B **58**, 8800 (1998).

[3] J. L. Peng *et al.,* Phys. Rev. B **55**, R6145 (1997).

[4] Q. Huang *et al.,* Nature (London) **347**, 369 (1990).

[5] D. H. Wu *et al.,* Phys. Rev. Lett. **70**, 85 (1993).

[6] B. Stadlober *et al.,* Phys. Rev. Lett. **74**, 4911 (1995); D. Einzel and R. Hackl, J. Raman Spectrosc. **27**, 307 (1996).

[7] J. D. Kokales *et al.,* Phys. Rev. Lett. **85**, 3696 (2000).

[8] R. Prozorov *et al.,* Phys. Rev. Lett. **85**, 3700 (2000).

[9] N. P. Armitage *et al.,* Phys. Rev. Lett. **86**, 1126 (2001).

[10] T. Sato *et al.,* Science **291**, 1517 (2001).

[11] C. C. Tsuei and J. R. Kirtley, Phys. Rev. Lett. **85**, 182 (2000).

[12] J. L. Peng *et al.,* Physica (Amsterdam) **177C**, 79 (1991).

[13] G. Blumberg *et al.,* Phys. Rev. B **49**, 13 295 (1994).

[14] S. B. Dierker *et al.,* Phys. Rev. Lett. **50**, 853 (1983); R. Hackl, R. Kaiser, and S. Schicktanz, J. Phys. C **16**, 1729 (1983).

[15] M. V. Klein and S. B. Dierker, Phys. Rev. B **29**, 4976 (1984).

[16] T. P. Devereaux and D. Einzel, Phys. Rev. B **51**, 16 336 (1995).

[17] N. P. Armitage *et al.,* Phys. Rev. Lett. **87**, 147003 (2001).

[18] R. Hlubina and T. M. Rice, Phys. Rev. B **51**, 9253 (1995).

[19] M. R. Norman *et al.,* Nature (London) **392**, 157 (1998); Phys. Rev. Lett. **79**, 3506 (1997).

[20] Z-X. Shen and J. R. Schrieffer, Phys. Rev. Lett. **78**, 1771 (1997).

[21] For the simplest nearest neighbor tight binding approximation the minimum contribution to the A_{1g} channel comes from the proximity of the $(\pi, 0) \rightarrow (0, \pi)$ and the equivalent diagonals.

[22] S. L. Cooper *et al.,* Phys. Rev. B **37**, 5920 (1988); **38**, 11 934 (1988).

[23] T. Staufer *et al.,* Phys. Rev. Lett. **68**, 1069 (1992).

[24] X. K. Chen *et al.,* Phys. Rev. Lett. **73**, 3290 (1994).

[25] T. P. Devereaux *et al.,* Phys. Rev. Lett. **72**, 396 (1994).

[26] M. Kang *et al.,* Phys. Rev. Lett. **77**, 4434 (1996).

[27] G. Blumberg *et al.,* Science **278**, 1427 (1997); J. Phys. Chem. Solids **59**, 1932 (1998).

[28] H. L. Liu *et al.,* Phys. Rev. Lett. **82**, 3524 (1999).

[29] M. T. Beal-Monod, J. B. Bieri, and M. Maki, Europhys. Lett. **40**, 201 (1997); **41**, 345 (1998).

[30] R. Nemetschek *et al.,* Eur. Phys. J. B **5**, 495 (1998).

[31] A. P. Kampf and T. P. Devereaux, Phys. Rev. B **56**, 2360 (1997).

[32] A. Chubukov, Europhys. Lett. **44**, 655 (1997).

[33] J. Schmalian *et al.,* Phys. Rev. Lett. **80**, 3839 (1998).

[34] L. B. Ioffe and A. J. Millis, Phys. Rev. B **58**, 11 631 (1998).

[35] D. Manske *et al.,* Phys. Rev. B **62**, 13 922 (2000).

[36] E. J. Singley *et al.,* Phys. Rev. B **64**, 224503 (2001).

[37] S. Uchida *et al.,* Phys. Rev. B **43**, 7942 (1991).